Am J Physiol Cell Physiol 308: C229–C236, 2015.
First published November 19, 2014; doi:10.1152/ajpcell.00315.2014.

CALL FOR PAPERS | *Physical Biology of Cancer*

The thrombotic potential of circulating tumor microemboli: computational modeling of circulating tumor cell-induced coagulation

Kevin G. Phillips,[1]* Angela M. Lee,[2]* Garth W. Tormoen,[1] Rachel A. Rigg,[1] Anand Kolatkar,[3] Madelyn Luttgen,[3] Kelly Bethel,[4] Lyudmila Bazhenova,[5] Peter Kuhn,[3] Paul Newton,[2] and Owen J. T. McCarty[1,6]

[1]*Department of Biomedical Engineering, School of Medicine, Oregon Health & Science University, Portland, Oregon;* [2]*Department of Aerospace and Mechanical Engineering, Viterbi School of Engineering, University of Southern California, Los Angeles, California;* [3]*Department of Biological Sciences, University of Southern California, Los Angeles, California;* [4]*Scripps Clinic Medical Group, Scripps Clinic, La Jolla, California;* [5]*University of California San Diego Moores Cancer Center, San Diego, California; and* [6]*Department of Cell, Developmental and Cancer Biology, School of Medicine, Oregon Health & Science University, Portland, Oregon*

Submitted 19 September 2014; accepted in final form 13 November 2014

Phillips KG, Lee AM, Tormoen GW, Rigg RA, Kolatkar A, Luttgen M, Bethel K, Bazhenova L, Kuhn P, Newton P, McCarty OJ. The thrombotic potential of circulating tumor microemboli: computational modeling of circulating tumor cell-induced coagulation. *Am J Physiol Cell Physiol* 308: C229–C236, 2015. First published November 19, 2014; doi:10.1152/ajpcell.00315.2014.— Thrombotic events can herald the diagnosis of cancer, preceding any cancer-related clinical symptoms. Patients with cancer are at a 4- to 7-fold increased risk of suffering from venous thromboembolism (VTE), with ~7,000 patients with lung cancer presenting from VTEs. However, the physical biology underlying cancer-associated VTE remains poorly understood. Several lines of evidence suggest that the shedding of tissue factor (TF)-positive circulating tumor cells (CTCs) and microparticles from primary tumors may serve as a trigger for cancer-associated thrombosis. To investigate the potential direct and indirect roles of CTCs in VTE, we characterized thrombin generation by CTCs in an interactive numerical model coupling blood flow with advection-diffusion kinetics. Geometric measurements of CTCs isolated from the peripheral blood of a lung cancer patient prior to undergoing lobectomy formed the basis of the simulations. Singlet, doublet, and aggregate circulating tumor microemboli (CTM) were investigated in the model. Our numerical model demonstrated that CTM could potentiate occlusive events that drastically reduce blood flow and serve as a platform for the promotion of thrombin generation in flowing blood. These results provide a characterization of CTM dynamics in the vasculature and demonstrate an integrative framework combining clinical, biophysical, and mathematical approaches to enhance our understanding of CTCs and their potential direct and indirect roles in VTE formation.

lung cancer; venous thromboembolism; circulating tumor microemboli; Navier-Stokes equation; advection-diffusion equation; coagulation; tissue factor

THE ASSOCIATION of cancer and cancer metastasis with the blood coagulation system has been observed for over a century (18, 22). Tumor cells have been shown to express tissue factor (TF) in vivo, and such tumor cells are associated with accelerated cancer progression and metastasis in experimental models (12, 13). Tissue factor is a receptor and enzyme cofactor of the coagulation factor (F) VII(a). In complex, TF-FVII(a) activates the extrinsic coagulation cascade leading to the formation of thrombin, which, through its protease activity, can polymerize soluble fibrinogen to insoluble fibrin. Fibrin, acting in concert with platelets, forms a hemostatic plug to halt bleeding outside blood vessels at sites of vascular injury, while thrombin generation and fibrin formation within blood vessels results in thrombosis, leading to cardiovascular complications such as pulmonary embolism, myocardial infarction, and stroke (7).

In metastatic cancer, the presence of TF-positive circulating tumor cells (CTCs) in the circulation may promote thrombin generation and fibrin formation leading to pathological thrombus formation. The incidence of thrombosis in cancer is known to correlate with cancer type and tissue of origin, suggesting that specific aspects of cancer cells may play a role in thrombus formation (3). In vitro, TF-positive epithelial cancer cells have been shown to initiate blood coagulation, while blocking TF function in these cells can reverse this effect, providing evidence that the expression of TF by cancer cells may play a pivotal role in promoting blood coagulation (2, 10, 26). Despite evidence that suggests that CTCs are present in the blood of patients across a multitude of epithelial carcinomas (1, 5), the role of CTCs in cancer-associated thrombosis is poorly understood.

To characterize thrombin formation by TF-positive CTCs, we developed a numerical model coupling blood flow with advection-diffusion kinetics of thrombin generation on the surface of CTCs. Clinical measurements on CTCs identified in the peripheral blood of a lung cancer patient served as the biophysical input for these simulations. Using the high-definition (HD) CTC assay (11), we investigated CTC populations in a lung cancer patient with a T3N0M0-staged adenocarcinoma before, during, and after pulmonary lobectomy. The T3N0M0 staging denotes a tumor mass $>$ 7 cm diameter, N0 = no regional lymph node metastasis, and M0 = no distant metastasis. Biophysical parameters of CTCs were measured using noninterferometric quantitative phase microscopy (NIQPM) (19).

* K. G. Phillips and A. M. Lee share first authorship and contributed equally to this work.

Address for reprint requests and other correspondence: O. McCarty, Dept. of Biomedical Engineering, Oregon Health & Science Univ., Portland, OR 97239 (e-mail: mccartyo@ohsu.edu; newton@usc.edu; pkuhnn@usc.edu).

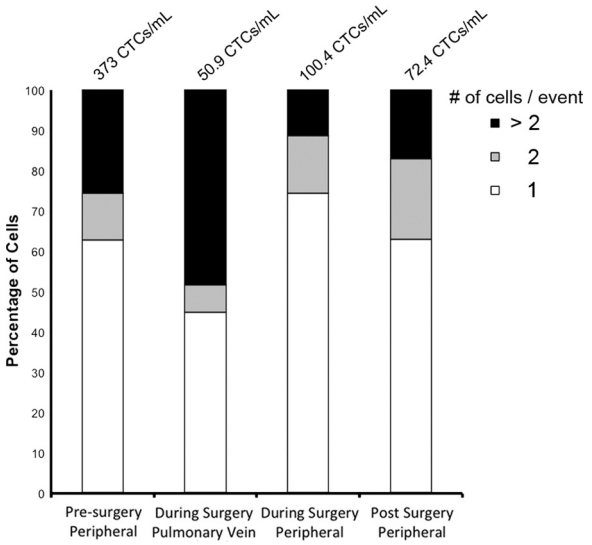

Fig. 1. Circulating tumor cell (CTC) populations observed at each clinical visit. Blood draws were taken from the peripheral venous before, during, and at follow-up to pulmonary lobectomy. During surgery, blood was sampled from the pulmonary vein draining the surgical site. CTCs were classified immunofluorescently using the high-definition (HD) CTC assay. CTCs were classified as cytokeratin positive, DAPI positive, or CD45 negative.

Simulations were designed to mimic the bifurcated vascular beds within the pulmonary circulation. We investigated thrombin generation dynamics as a function of flow, CTC size, and CTC clustering (circulating tumor microemboli, CTM). This work substantially adds to previous models and simulations of coagulation processes (9) by utilizing physiologically relevant measurements of CTCs to characterize the role of thrombin generation at the CTC cell surface within the bloodstream.

MATERIALS AND METHODS

HD-CTC and leukocyte identification and characterization. A 45-yr-old female gave written informed consent at the UCSD Moores Cancer Center, as approved by the internal review board. The patient, a nonsmoker, presented with hemoptysis and was found to have an 8-cm right lower lobe mass. The mass was removed through surgical lobectomy and, upon pathological examination, was found to be a well differentiated adenocarcinoma of the bronchoalveolar type. There was no evidence of vascular invasion. Following surgery, the patient received adjuvant chemotherapy for 2 mo. No recurrence was detected at a 3-yr follow-up examination.

To investigate potential alterations in circulating tumor cells resulting from surgical intervention, blood draws were collected before, during, and immediately following surgery. At each draw, 8 ml of peripheral blood was collected in a rare cell blood collection tube (Streck, Omaha, NE) and processed within 24 h after phlebotomy. CTCs were identified using the HD-CTC method, as previously reported (11). Briefly, the HD-CTC isolation and characterization technique consists of red blood cell lysis, after which nucleated cells are attached as a monolayer to custom-made glass slides. Slides are subsequently incubated with antibodies against cytokeratins (CK) 1, 4–8, 10, 13, 18, and 19 and CD45 with Alexa 647-conjugated secondary antibody; nuclei were counterstained with DAPI.

For HD-CTC identification, an automated digital fluorescence microscope was used to identify putative HD-CTCs. Fluorescence images of CTC candidates were then presented to a hematopathologist for interpretation. Cells were classified as HD-CTCs if they were both CK-positive and CD45-negative, contained an intact DAPI nucleus without identifiable apoptotic changes or a disrupted appearance, and were morphologically distinct from surrounding leukocytes. Leukocytes were classified according to a CK-negative, CD45-positive, or DAPI-positive fluorescence profile (Fig. 4).

Cartesian coordinates for each HD-CTC on a slide were generated from a fixed fiduciary marking and used to relocate the cells of interest for optical measurements and computational mesh generation (Fig. 4). Leukocytes located in the same field of view of HD-CTCs were selected at random for quantitative comparison to the HD-CTC population.

Noninterferometric quantitative phase microscopy. Cellular density of CTCs was quantified using NIQPM on an upright optical microscope (Axio Imager; Carl Zeiss, Gottingen, Germany) equipped with a ×63/1.4 numerical aperture (NA) oil immersion objective and an air-coupled condenser lens providing Köhler illumination at an NA of 0.1. Through-focus bright field imagery of the cells was acquired

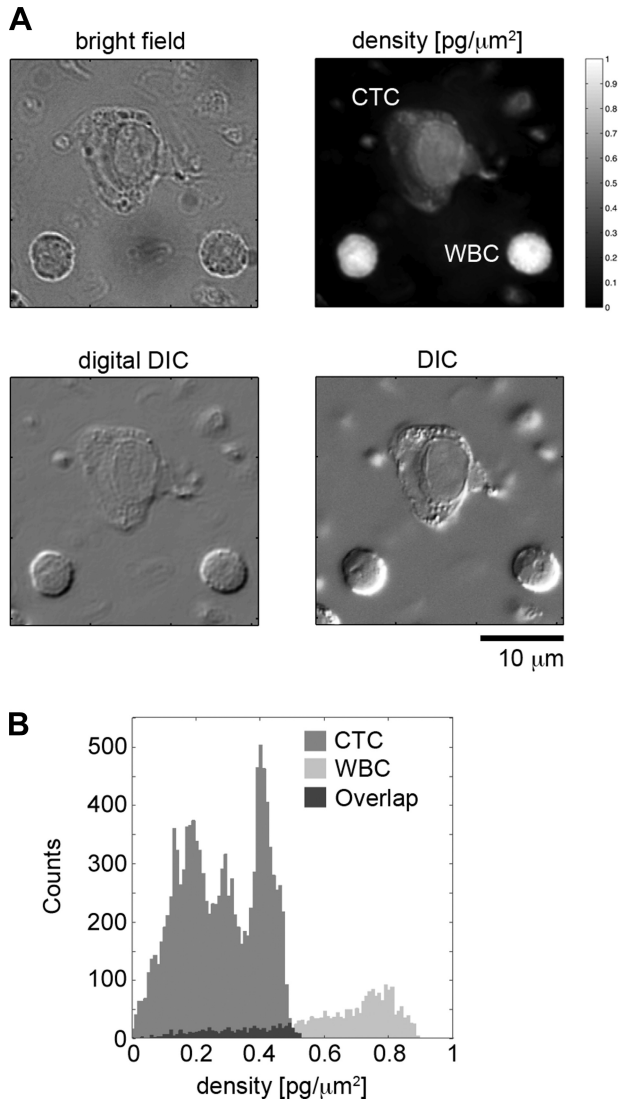

Fig. 2. Noninterferometric quantitative phase microscopy (NIQPM). The subcellular density organization of CTCs was quantified using NIQPM. *A*: NIQPM uses through-focus bright field images as input to a wave model to determine the density map. The density map is checked for self-consistency through the numerical generation of a digital differential interference contrast (DIC) image and validation against the true DIC image. *B*: density maps corresponding to each cell type are binned into histograms to elucidate the differential organization of the density among CTCs and white blood cells (WBCs).

using an illumination wavelength of 540 ± 20 nm. Bright field images of the sample field were recorded with a charge-coupled device camera (AxioCam MRc5 12-bit camera; Carl Zeiss) under software control by Slidebook 5.5 (Intelligent Imaging Innovations, Denver, CO). Through-focus images were acquired in 0.1-μm increments over a 10-μm range along the optical axis. These images formed the input to a transport of intensity equation solver to extract phase of transmitted waves through the sample from intensity measurements (6, 16).

Knowledge of the phase enables the enumeration of the projected mass density, defined as the sum of the three-dimensional density along the optical axis of the microscope, through the following relationship (16, 19):

$$\rho(x,y) = \frac{\lambda\varphi(x,y)}{2\pi\alpha}\left[\mathrm{pg}/\mu\mathrm{m}^2\right] \quad (1)$$

Here $\rho(x,y)$ denotes the projected mass density, λ is the illumination wavelength, and α is the specific refraction increment of the cell solids (~0.2 [ml/g]). The correct mass density map is verified by computing the digital differential interference contrast (DIC) image as previously described (6, 16) (Fig. 2*A*).

To examine cellular dry mass density parameters, histograms of CTC subcellular density maps were constructed with bin sizes of 0.01 over the range of 0 to 2 [pg/μm^2] for each cell (6). These histograms were then normalized into probability density functions for each cell type. From the image segmentation and histogram procedures, four parameters were determined: area, total dry mass, dry mass density mean, and standard deviation of the dry mass density, (Figs. 2*B* and 3*B*). Leukocytes located in the same field of view as HD-CTCs were selected at random to serve as a control population, (Fig. 3, *A* and *B*).

CTC vascular transport and feed-forward thrombin generation: numerical simulations in COMSOL. Numerical simulations were performed using the COMSOL Multiphysics software package (http://www.comsol.com). This package utilizes adaptive finite-element mesh generation to determine numerical solutions to coupled partial differential equations with prescribed initial and boundary conditions.

The computational domain of the model was chosen to represent the branching arterioles of the pulmonary circulation. HD-CTCs, imaged under DIC, were then incorporated into the computational domain of the model through triangulation (Fig. 4). CTC singlets, doublets, and CTM were investigated in the model.

We used the incompressible Navier-Stokes equations (15) to simulate blood flow coupled to a reaction-diffusion system to model thrombin generation. COMSOL uses a moving triangular mesh to track the position of the fluid-fluid interface. The fluid outside the cell boundary represents blood, and the fluid inside represents the homogenized (i.e., spatially averaged) inner contents of the cell. The concentration fields of thrombin generation associated with each cell are modeled via the advection-diffusion equations coupled to the Navier-Stokes solver, with reaction kinetics initiated on the outer cell surface.

The model incorporates CTC membrane deformability by imposing a surface tension criterion at the interface between the two fluids (outer cell/inner cell). The surface tension is inversely proportional to the deformability of the cell, meaning a lower value of surface tension results in a more deformable interface. The fluid flow physics we specify in our model is a laminar two-phase flow, which models the laminar flow between two immiscible fluids. Boundary conditions at the blood vessel walls are the viscous no-slip conditions, and at the cell wall, the velocity of the blood is equal to the velocity of the cell wall boundary. Boundary conditions for the concentration field at the vessel wall and cell walls are the no penetration conditions (Neumann boundary conditions).

Parameters of the model were chosen to match those found in the literature. The density (ρ) and dynamic viscosity (μ) for the fluid velocity field are chosen to match values for blood at body tempera-

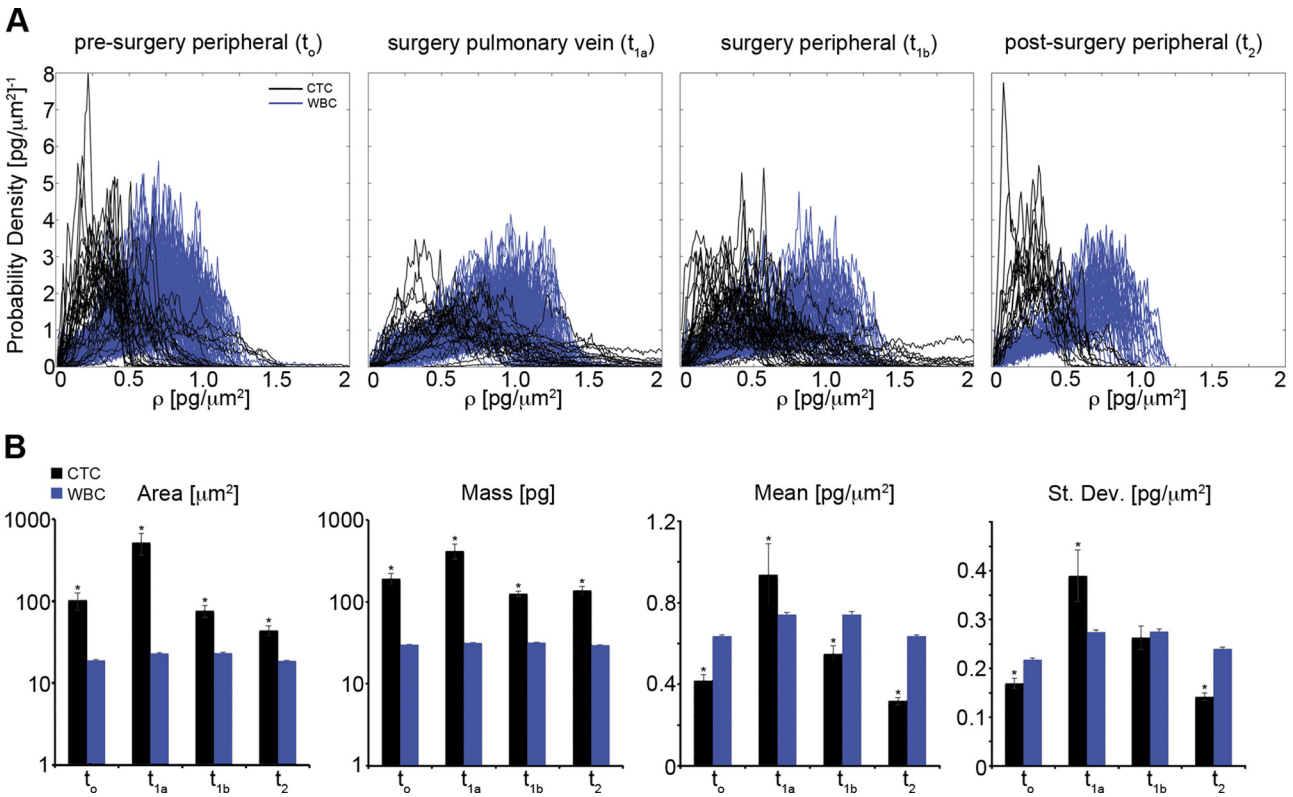

Fig. 3. Subcellular density metrics of CTCs and WBCs across clinical time points. Throughout, t_o denotes presurgery peripheral, t_{1a} denotes during surgery pulmonary vein, t_{1b} denotes during surgery peripheral, t_2 denotes postsurgery peripheral. *A*: probability density functions of the subcellular density measured for CTCs and WBCs. *B*: biophysical properties determined from both image segmentation and the first- and second-order statistics of the probability density functions. St. Dev., standard deviation. *$P < 0.05$ with respect to WBCs.

ture: $\rho = 1{,}060$ kg/m^3 and $\mu = 3 \times 10^{-3}$ Pa·s. Blood flow assumes a parabolic flow profile (Poiseuille flow) at the inlet, and a pressure gradient field drives the flow. The density of the cell was determined using NIQPM-based measurements. The dynamic viscosity of the cell is set to $\mu_{cell} = 1.36$ Pa·s, which is three orders of magnitude greater than that of blood. We used reported diffusion coefficients of $\sim 2 \times 10^{-7}$ cm^2/s for coagulation factors in the blood, ~ 10 μm^2/s for thrombin (4).

Statistical analysis. For NIQPM studies, the Jarque-Bera test was used to evaluate normality of all parameters. One-way analysis of variance with Bonferroni *post hoc* correction was used to assess statistical significance among parameters across multiple normally distributed cell parameters. The Kruskal-Wallis test was used to assess significance among non-normally distributed parameters. $P \leq 0.05$ was considered significant.

RESULTS

Biophysical characterization of the subcellular architecture of CTCs obtained before, during, and after pulmonary lobectomy. To obtain a clinical snapshot of CTC dynamics, we utilized the HD-CTC assay to both count and visualize CTCs in blood draws obtained before, during, and after pulmonary lobectomy. The HD-CTC assay revealed that CTCs circulated at concentrations of 373 [CTCs/ml] (presurgery, peripheral), 50.9 [CTCs/ml] (during surgery, pulmonary vein), 100.4 [CTCs/ml] (during surgery, peripheral), and 72.4 [CTCs/ml] (postsurgery, peripheral). Moreover, we observed the presence of circulating singlet, doublet, and CTM aggregate (>2 cells/event) CTCs at each clinical time point (Fig. 1), despite the N0M0 staging of the tumor. The highest percentage of clusters was observed in blood draws obtained during surgery in samples from the pulmonary vein draining the surgical site (Fig. 1).

To evaluate the biophysical properties of CTCs across clinical time points, we utilized label-free quantitative imagery, NIQPM, to determine the spatial dependence of the projected dry mass density (Fig. 2). Dry mass density maps were then converted to histograms to elucidate the subcellular density distribution (Fig. 3*A*). Leukocytes from the same field of view were selected at random and similarly quantified as a positive control across the clinical time points. Next, the total cellular dry mass, the mean dry mass density, density fluctuations, and area were quantified for both CTCs and white blood cells (Fig. 3*B*).

Area, mass, mean density, and the standard deviation of the density were conserved across clinical time points, indicating the absence of cellular alterations arising from blood collection and preparation for imaging. The physical properties of CTCs obtained in peripheral blood draws were conserved across clinical time points, while those obtained during surgery from the pulmonary vein had increased area, dry mass, dry mass density, and density fluctuations (Fig. 3*B*).

Numerical evaluation of the procoagulant activity of CTCs under Poiseuille flow. To define the role of CTC geometry in regulating the physical biology of the procoagulant activity of CTCs, a numerical model was constructed to model two-dimensional (2D) CTC vascular transport. Subsequent to HD-CTC immunofluorescent identification, CTCs were imaged under DIC microscopy to visualize their full physical extent (Fig. 4). A computational mesh consisting of 1,900, 1,210, and 4,165 triangular domain elements for singlet, doublet, and

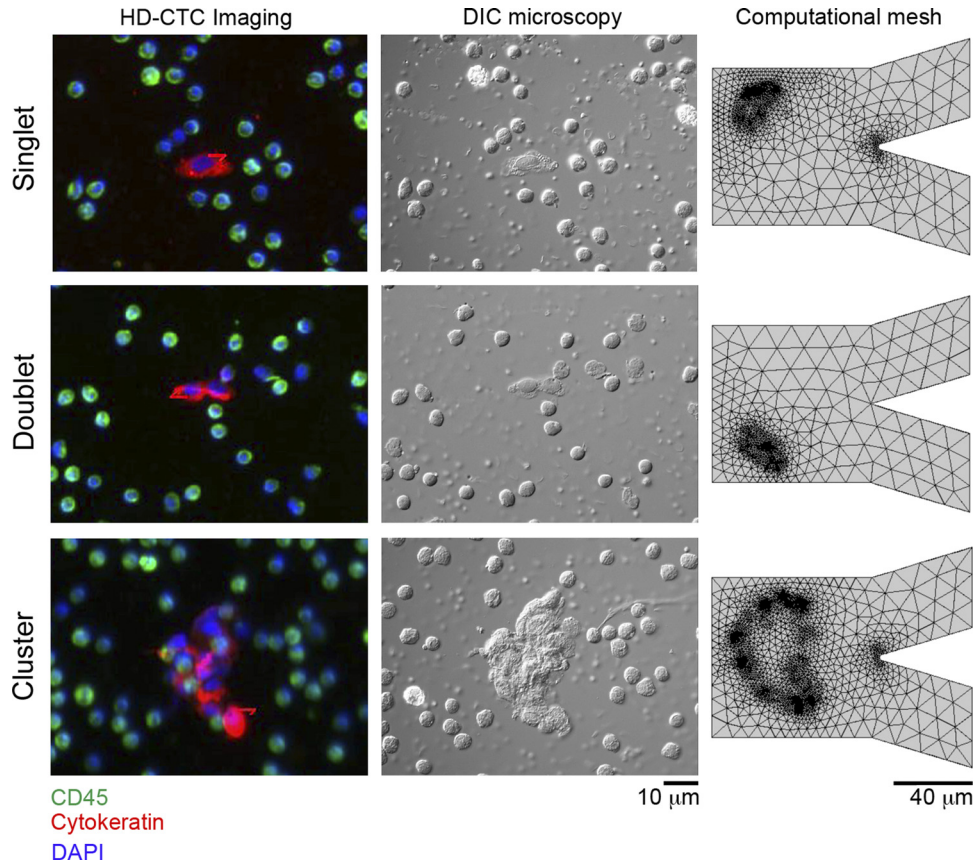

Fig. 4. Image segmentation for fluid dynamics simulations. CTCs are first identified immunofluorescently using the HD-CTC assay (*left*) and then imaged under differential interference contrast to delineate the full borders of the cell (*middle*). A computational mesh consisting of 1,900 (singlet), 1,210 (doublet), and 4,165 (cluster) domain elements is then generated to model CTC propagation in a bifurcated vascular geometry (*right*).

cluster CTC geometries, respectively, was then generated, (Fig. 4). To model the vasculature of the lung, CTC transport was modeled numerically in an arteriole branching into two 40-μm channels from a single 80-μm channel (Fig. 4).

Our numerical model of CTC transport through the vasculature demonstrated that large clusters are capable of vascular plugging while smaller clusters tumble during flow and thus experience multiple interactions with the vessel wall. We observed that CTC clusters were large enough to temporally occlude the vessel juncture (Fig. 5), which slows the velocity field down enough to enable an increase in local thrombin generation levels (Fig. 6). This was further evidenced by the decreasing values of thrombin flux as a function of CTM size (Fig. 7). These conclusions are robust to changes in model parameters.

DISCUSSION

The primary cause of cancer-related death is due to metastasis, the spread and subsequent colonization of distant tissues by cancer cells from the primary tumor (18). The presence of circulating tumor cells (CTCs) in the vasculature has been implicated in the metastatic cascade of epithelial tumors, as CTCs accompany metastatic disease across all major types of carcinomas. Recently, the discovery that the number of CTCs in peripheral blood is predictive of overall survival in non-small cell lung cancer (NSCLC) has suggested that CTC enumeration may serve as an additional biomarker for monitoring, staging, and prognosticating NSCLC (14).

Approximately 3% of lung cancer patients develop VTE within 2 yr of diagnosis, with the occurrence of VTE conferring a higher risk of death. With the diagnosis of 1.6 million new cases of lung cancer each year, 220,000 of these occurring in the US, the development of VTE in lung cancer patients represents a significant source of morbidity and mortality (21). Despite the ongoing presence of VTE in lung and other epithelial cancers, the pathomechanisms underlying cancer-associated VTE remain poorly understood.

To reduce the burden and effects of VTE among patients with cancer, it is important to identify those individuals at highest risk of VTE who would benefit from thromboprophylaxis. Epidemiological and clinical studies have focused on identifying patient parameters that are predictive of symptomatic VTE (8); these parameters include the site of the cancer, prechemotherapy platelet count, hemoglobin levels, prechemotherapy leukocyte count, and body mass index. Furthermore, it is appreciated that lung cancer patients receiving chemotherapy, in the absence of surgical intervention, are eight times more likely to develop pulmonary embolism (PE), whereas those patients who received surgery are three times more likely to develop PE compared with cancer-free controls (25). Together with the finding that CTCs can predict overall survival in lung cancer, these clinical vignettes suggest a role for CTCs in the onset and development of pathological thrombi.

To date, guidelines for the management of VTE in cancer have yet to take into account CTC enumeration, owing in part to the difficulty of accessing these cells. Here, we utilized the HD-CTC assay and label-free microscopy approaches to evaluate the role of CTCs in a model of intravascular thrombin generation. Using the HD-CTC assay we obtained a clinical portrait of CTC dynamics in a lung patient undergoing lobectomy. We observed >20 CTCs in blood draws at all time points, despite the N0M0 staging of the tumor. To investigate the thrombotic potential of these cells, we developed a numerical model coupling advection-diffusion kinetics with CTC

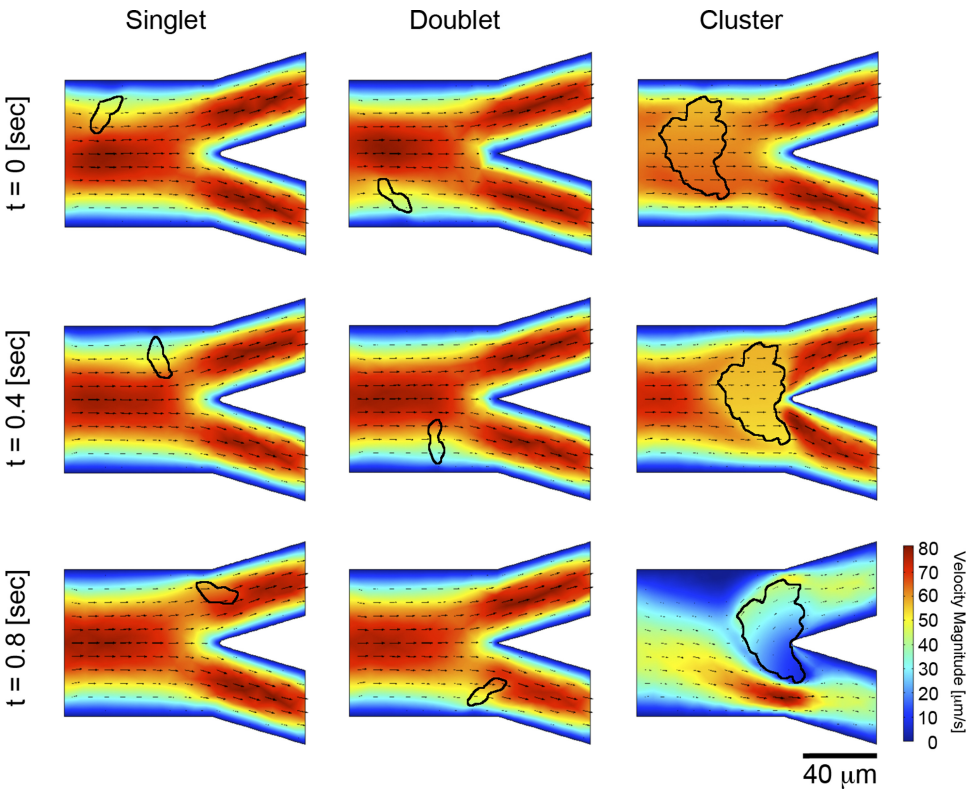

Fig. 5. Fluid dynamic simulations of CTC dynamics under flow. CTCs are propagated under parabolic flow in a bifurcated vascular geometry with no-slip boundary conditions. The blood velocity field (concentration surface plot) with velocity vectors (black arrows) is presented with CTC geometry superimposed. Positions of each CTC within the model vasculature are reported for $t = 0$, 0.4, and 0.8 s.

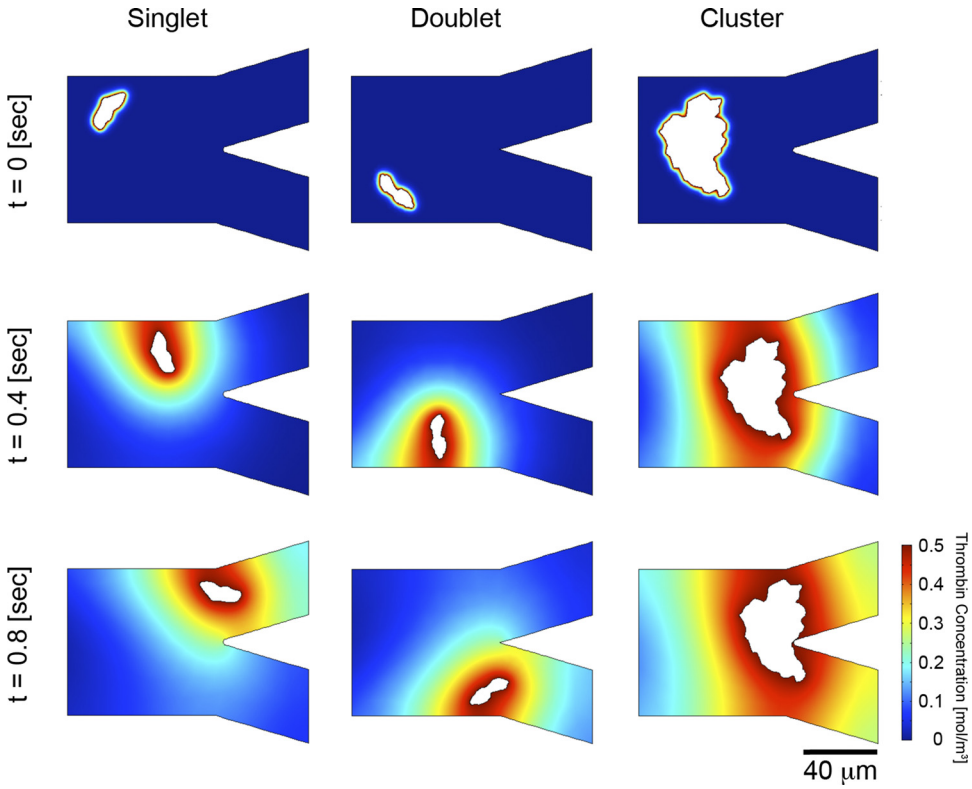

Fig. 6. Simulation of thrombin generation initiated by CTCs under flow. Advection-diffusion simulation of thrombin concentration fields with diffusion coefficient of 10 $\mu m^2/s$. Thrombin levels are shown to propagate outward from the CTC and collect at vessel walls.

transport under Poiseuille flow conditions through a branched vascular geometry indicative of lung capillary beds. This model builds on our previous model of thrombin generation that relied on treating each cell as a point particle (9), and thus was unable to account for cell shape or deformability. Moreover, our previous model was constrained by inviscid boundary conditions (9), which allowed us to use analytical methods (Green's function formulation) to study concentration fields

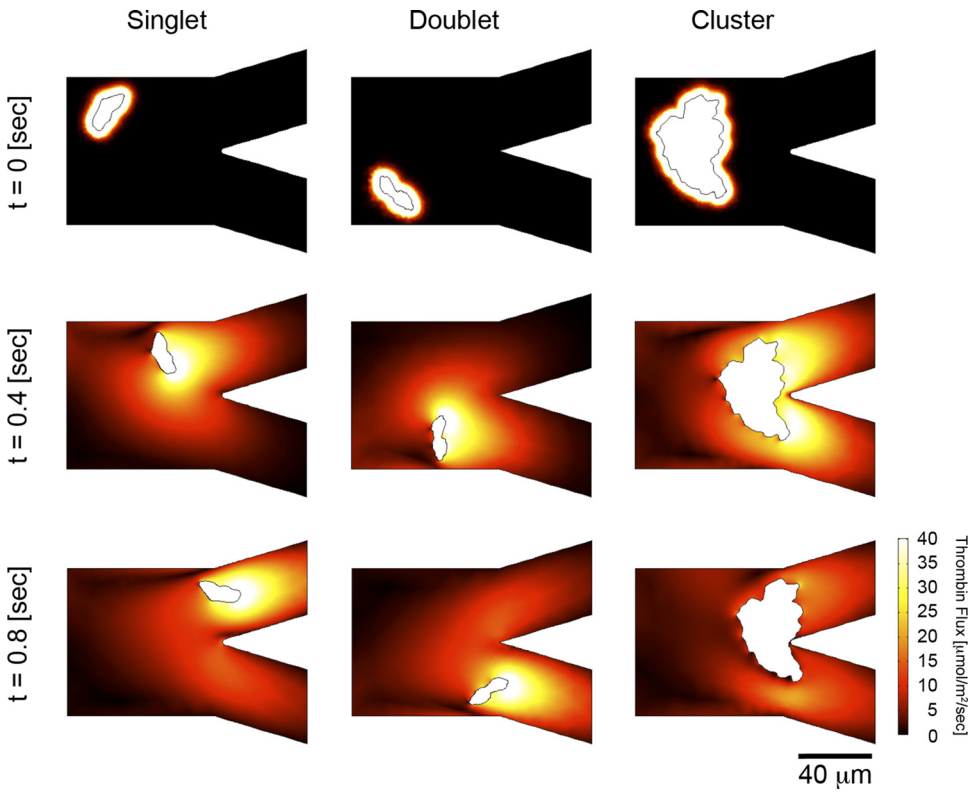

Fig. 7. Simulation of thrombin gradient away from CTCs under flow. Advection-diffusion simulation of thrombin flux with diffusion coefficient of 10 $\mu m^2/s$. Thrombin flux is shown to propagate outward from the CTC whereupon it interacts strongly with the flow field, resulting in fluxes projected along flow contours.

generated by point particles in uniform flow. The model presented in the current study overcomes several limitations as follows: *1*) CTCs are treated as 2D objects, with physical parameters established from patient-derived CTCs; *2*) CTCs are deformable; *3*) the boundary conditions on both CTCs and walls are viscous; *4*) the vessel geometries are branched; *5*) inclusion of viscous boundary conditions allows the study of a Poiseuille flow field (parabolic), with boundary layers resolved; and *6*) a COMSOL Multiphysics package was used, which produces a deforming finite-element mesh to resolve the flow around the CTCs and walls, and track the concentration fields. Our simulations demonstrate that singlet CTCs and small clusters are mobile sources of thrombin generation. Larger CTM can be temporarily slowed by the vascular junctures resulting in the *1*) reduction of the velocity field (Fig. 5) and *2*) a local increase in thrombin generation (Fig. 6). This potentially pathological thrombin buildup could provide a physical basis for VTE in cancer.

While correlative studies are invaluable in identifying new approaches in the clinic, probing the physics of cancer (20) to elucidate predictive models of cancer-associated thrombosis is also essential to the development of new strategies to address VTE. Our limited case report on a single patient suggests that testing the hypothesis that CTC count (9, 22–24) and CTC geometry (5, 17, 19) could potentially aid in stratifying patients for continued thromboprophylaxis following surgery and/or concurrent with chemotherapy. Further clinical data will be required to establish the role of CTCs in VTE.

GRANTS

This work was supported by the National Institutes of Health under National Cancer Institute Grant U54CA143906 (P. Kuhn, O. J. T. McCarty, P. Newton) and National Heart, Lung, and Blood Institute Grant R01HL101972 (O. J. T. McCarty) and the American Heart Association (12PRE11930019 to G. W. Tormoen and 13EIA12630000 to O. J. T. McCarty) and a Medical Research Foundation Early Clinical Investigator Award (K. G. Phillips). A. M. Lee and G. W. Tormoen are ARCS scholars.

DISCLOSURES

No conflicts of interest, financial or otherwise, are declared by the author(s).

AUTHOR CONTRIBUTIONS

K.G.P., A.M.L., R.A.R., A.K., M.L., and L.B. performed experiments; K.G.P., A.M.L., G.W.T., R.A.R., A.K., M.L., K.B., L.B., P.K., P.N., and O.J.T.M. analyzed data; K.G.P., A.M.L., G.W.T., and K.B. interpreted results of experiments; K.G.P. and A.M.L. prepared figures; K.G.P., A.M.L., G.W.T., R.A.R., P.N., and O.J.T.M. drafted manuscript; K.G.P., A.M.L., G.W.T., R.A.R., A.K., M.L., K.B., L.B., P.K., P.N., and O.J.T.M. approved final version of manuscript; K.B., L.B., P.K., P.N., and O.J.T.M. edited and revised manuscript; L.B., P.K., P.N., and O.J.T.M. conception and design of research.

REFERENCES

1. **Allard WJ, Matera J, Miller MC, Repollet M, Connelly MC, Rao C, Tibbe AG, Uhr JW, Terstappen LW.** Tumor cells circulate in the peripheral blood of all major carcinomas but not in healthy subjects or patients with nonmalignant diseases. *Clin Cancer Res* 10: 6897–6904, 2004.
2. **Berny-Lang MA, Aslan JE, Tormoen GW, Patel IA, Bock PE, Gruber A, McCarty OJ.** Promotion of experimental thrombus formation by the procoagulant activity of breast cancer cells. *Phys Biol* 8: 015014, 2011.
3. **Blom JW, Doggen CJ, Osanto S, Rosendaal FR.** Malignancies, prothrombotic mutations, and the risk of venous thrombosis. *JAMA* 293: 715–722, 2005.
4. **Bodner T, Sequeira A.** Numerical simulation of the coagulation dynamics of blood. *Comput Math Methods Med* 9: 83–104, 2008.
5. **Cho EH, Wendel M, Luttgen M, Yoshioka C, Marrinucci D, Lazar D, Schram E, Nieva J, Bazhenova L, Morgan A, Ko AH, Korn WM, Kolatkar A, Bethel K, Kuhn P.** Characterization of circulating tumor cell aggregates identified in patients with epithelial tumors. *Phys Biol* 9: 016001, 2012.
6. **Damania D, Subramanian H, Backman V, Anderson EC, Wong MH, McCarty OJ, Phillips KG.** Network signatures of nuclear and cytoplasmic density alterations in a model of pre and postmetastatic colorectal cancer. *J Biomed Opt* 19: 16016, 2014.
7. **Gomez K, McVey JH.** Tissue factor initiated blood coagulation. *Front Biosci* 11: 1349–1359, 2006.
8. **Khorana AA, Kuderer NM, Culakova E, Lyman GH, Francis CW.** Development and validation of a predictive model for chemotherapy-associated thrombosis. *Blood* 111: 4902–4907, 2008.
9. **Lee AM, Tormoen GW, Kanso E, McCarty OJ, Newton PK.** Modeling and simulation of procoagulant circulating tumor cells in flow. *Front Oncol* 2: 108, 2012.
10. **Marchetti M, Diani E, ten Cate H, Falanga A.** Characterization of the thrombin generation potential of leukemic and solid tumor cells by calibrated automated thrombography. *Haematologica* 97: 1173–1180, 2012.
11. **Marrinucci D, Bethel K, Kolatkar A, Luttgen MS, Malchiodi M, Baehring F, Voigt K, Lazar D, Nieva J, Bazhenova L, Ko AH, Korn WM, Schram E, Coward M, Yang X, Metzner T, Lamy R, Honnatti M, Yoshioka C, Kunken J, Petrova Y, Sok D, Nelson D, Kuhn P.** Fluid biopsy in patients with metastatic prostate, pancreatic and breast cancers. *Phys Biol* 9: 016003, 2012.
12. **McCarty OJ, Mousa SA, Bray PF, Konstantopoulos K.** Immobilized platelets support human colon carcinoma cell tethering, rolling, and firm adhesion under dynamic flow conditions. *Blood* 96: 1789–1797, 2000.
13. **Mueller BM, Ruf W.** Requirement for binding of catalytically active factor VIIa in tissue factor-dependent experimental metastasis. *J Clin Invest* 101: 1372–1378, 1998.
14. **Nieva J, Wendel M, Luttgen MS, Marrinucci D, Bazhenova L, Kolatkar A, Santala R, Whittenberger B, Burke J, Torrey M, Bethel K, Kuhn P.** High-definition imaging of circulating tumor cells and associated cellular events in non-small cell lung cancer patients: a longitudinal analysis. *Phys Biol* 9: 016004, 2012.
15. **Pedley TJ.** *The Fluid Mechanics of Large Blood Vessels*. New York: Cambridge Univ. Press, 1980, p. xv, 446 p.
16. **Phillips KG, Baker-Groberg SM, McCarty OJ.** Quantitative optical microscopy: measurement of cellular biophysical features with a standard optical microscope. *J Vis Exp* 86: 2014; doi: 10.3791/50988.
17. **Phillips KG, Kolatkar A, Rees KJ, Rigg R, Marrinucci D, Luttgen M, Bethel K, Kuhn P, McCarty OJ.** Quantification of cellular volume and sub-cellular density fluctuations: comparison of normal peripheral blood cells and circulating tumor cells identified in a breast cancer patient. *Front Oncol* 2: 96, 2012.
18. **Phillips KG, Kuhn P, McCarty OJ.** Physical Biology in Cancer. 2. The physical biology of circulating tumor cells. *Am J Physiol Cell Physiol* 306: C80–C88, 2014.
19. **Phillips KG, Velasco CR, Li J, Kolatkar A, Luttgen M, Bethel K, Duggan B, Kuhn P, McCarty OJ.** Optical quantification of cellular mass, volume, and density of circulating tumor cells identified in an ovarian cancer patient. *Front Oncol* 2: 72, 2012.
20. **Physical Sciences-Oncology Centers N, Agus DB, Alexander JF, Arap W, Ashili S, Aslan JE, Austin RH, Backman V, Bethel KJ, Bonneau R, Chen WC, Chen-Tanyolac C, Choi NC, Curley SA, Dallas M, Damania D, Davies PC, Decuzzi P, Dickinson L, Estevez-Salmeron L, Estrella V, Ferrari M, Fischbach C, Foo J, Fraley SI, Frantz C, Fuhrmann A, Gascard P, Gatenby RA, Geng Y, Gerecht S, Gillies RJ, Godin B, Grady WM, Greenfield A, Hemphill C, Hempstead BL, Hielscher A, Hillis WD, Holland EC, Ibrahim-Hashim A, Jacks T, Johnson RH, Joo A, Katz JE, Kelbauskas L, Kesselman C, King MR, Konstantopoulos K, Kraning-Rush CM, Kuhn P, Kung K, Kwee B, Lakins JN, Lambert G, Liao D, Licht JD, Liphardt JT, Liu L, Lloyd MC, Lyubimova A, Mallick P, Marko J, McCarty OJ, Meldrum DR, Michor F, Mumenthaler SM, Nandakumar V, O'Halloran TV, Oh S, Pasqualini R, Paszek MJ, Philips KG, Poultney CS, Rana K, Reinhart-King CA, Ros R, Semenza GL, Senechal P, Shuler ML, Srinivasan S, Staunton JR, Stypula Y, Subramanian H, Tlsty TD, Tormoen GW, Tseng Y, van Oudenaarden A, Verbridge SS, Wan JC, Weaver VM, Widom J, Will C, Wirtz D, Wojtkowiak J, Wu PH.** A

physical sciences network characterization of nontumorigenic and metastatic cells. *Sci Rep* 3: 1449, 2013.
21. **Sorensen HT, Mellemkjaer L, Steffensen FH, Olsen JH, Nielsen GL.** The risk of a diagnosis of cancer after primary deep venous thrombosis or pulmonary embolism. *N Engl J Med* 338: 1169–1173, 1998.
22. **Tormoen GW, Haley KM, Levine RL, McCarty OJ.** Do circulating tumor cells play a role in coagulation and thrombosis? *Front Oncol* 2: 115, 2012.
23. **Tormoen GW, Recht O, Gruber A, Levine RL, McCarty OJ.** Phosphatidylserine index as a marker of the procoagulant phenotype of acute myelogenous leukemia cells. *Phys Biol* 10: 056010, 2013.
24. **Tormoen GW, Rugonyi S, Gruber A, McCarty OJ.** The role of carrier number on the procoagulant activity of tissue factor in blood and plasma. *Phys Biol* 8: 066005, 2011.
25. **van Herk-Sukel MP, Shantakumar S, Penning-van Beest FJ, Kamphuisen PW, Majoor CJ, Overbeek LI, Herings RM.** Pulmonary embolism, myocardial infarction, and ischemic stroke in lung cancer patients: results from a longitudinal study. *Lung* 191: 501–509, 2013.
26. **Welsh J, Smith JD, Yates KR, Greenman J, Maraveyas A, Madden LA.** Tissue factor expression determines tumour cell coagulation kinetics. *Int J Lab Hematol* 34: 396–402, 2012.